A High Visual Quality Color Image Reversible Data Hiding Scheme Based on B-R-G Embedding Principle and CIEDE2000 Assessment Metric

Yang Yang, Tianrui Zou, Genyan Huang, and Weiming Zhang

***Abstract*— Reversible data hiding methods for color images are investigated because of the popularity of color images. However, the traditional RDH methods for color images only take PSNR as the assessment metric and pursue a high PSNR value. To further consider the different subjective perception in the R, G, and B channels of the color image, this paper proposes a high visual quality color image reversible data hiding scheme based on the B-R-G embedding principle and the CIEDE2000 assessment metric. In this method, a double-layer least square prediction is proposed to satisfy the sorting requirement and maintain prediction accuracy, and then the B-R-G embedding principle is proposed to improve the visual quality of the marked color images based on the different visual perception in the three channels, and finally, a one-by-one embedding method is proposed to reduce the embedding distortion by maintaining the inter channel correlation. The experimental results show that the proposed method is superior to the state-of-the-art RDH methods for color images.**

***Index Terms*— Reversible data hiding, double-layer LS predictor, energy threshold, B-R-G embedding principle, one-by-one embedding method.**

I. Introduction

DATA hiding [1] embeds secret data into cover medium such as audio, video, and images in an imperceptible manner, and user can extract the embedded data from the marked medium. The data hiding method plays an important role in privacy protection. Data hiding techniques can be roughly divided into three categories of robust watermarking [2], [3] that can resist some attacks, fragile watermarking [4] that is no robustness against possible attacks, and finally, steganography [5] that has a strong undetectability and is able to resist steganalysis. Robust watermarking, fragile watermarking and steganography are mainly used for copyright protection to ensure the copyrights of the computerized portraits, the original cover medium integrity authentication and secret communication, respectively. However, robust watermarking, some fragile watermarking and steganography algorithms will irreversibly destroy the original cover medium in the process of data hiding. In some applications such as military, judicial, medical and other image authentication or labeling applications where it is necessary to losslessly recover the cover medium, such permanent distortion is strictly prohibited, and the original cover medium must be recovered accurately. To solve this issue, reversible data hiding (RDH) is proposed to losslessly recover the secret messages and the original cover medium. The RDH method using the image as the cover medium can be roughly divided into the gray RDH method and the color RDH method.

In this paper, a high visual quality color image RDH scheme based on the B-R-G embedding principle and CIEDE2000 assessment metric is proposed to further exploit the different visual perception among each channel and improve the visual quality through the B-R-G embedding principle. First, we propose a double-layer LS predictor for prediction. Second, we sort the prediction error sequences, and then use the energy threshold to select low energy pixels. Third, we use the B-R-G embedding principle to allocate the secret messages, and embed the messages by prediction error expansion (PEE).

The main contributions of this work are as follows: first, we propose B-R-G embedding principle according to the different visual perception in three channels to improve the visual quality of the marked color images. Second, we propose double-layer LS prediction by combining the characteristics of Rhombus prediction and local LS prediction to achieve the sorting requirement and maintain sufficient accuracy of prediction. Finally, we introduce a new embedding scheme by using the energy threshold and maintaining the inter channel correlation to reduce the embedding distortion.

The rest of this paper is organized as follows. We briefly introduce the related work in Section II. Section III introduces the image quality assessment metric of CIEDE2000. Section IV provides a detailed description of the proposed methods that contains prediction algorithms of a double-layer

Manuscript received April 8, 2020; revised September 24, 2020 and February 8, 2021; accepted May 15, 2021. Date of publication May 28, 2021; date of current version April 5, 2022. This work was supported in part by the Natural Science Foundation of China under Grant 61502007 and Grant 61572452, in part by the Natural Science Research Project of Anhui province under Grant 1608085MF125, in part by the NO. 58 China Post-Doctoral Science Foundation under Grant 2015M582015, and in part by the Backbone Teacher Training Program of Anhui University and the Doctoral Scientific Research Foundation of Anhui University under Grant J01001319. This article was recommended by Associate Editor P. Bestagini. *(Corresponding author: Yang Yang.)*

Yang Yang, Tianrui Zou, and Genyan Huang are with the School of Electronics and Information Engineering, Anhui University, Hefei 230601, China (e-mail: sky_yang@ahu.edu.cn).

Weiming Zhang is with the School of Information Science and Technology, University of Science and Technology of China, Hefei 230026, China (e-mail: zhangwm@ustc.edu.cn).

Color versions of one or more figures in this article are available at https://doi.org/10.1109/TCSVT.2021.3084676.

Digital Object Identifier 10.1109/TCSVT.2021.3084676

LS predictor, sorting and selecting the prediction-error sequence and the B-R-G embedding principle. Section V presents the experimental results, followed by the conclusion in Section VI.

II. Related Works

In this section, we will introduce the current common RDH algorithm and some studies on the Internationale Commission on Illumination(CIE) color space. Numerous RDH methods can be classified into two subclasses, namely the RDH methods based on gray images and the RDH methods based on color images. The former generally used the correlation between neighboring pixels to predict and generate a sharp histogram of prediction errors and then embedded messages by modifying the histogram, while in the latter, the image can be split into three interconnected gray images, and in each gray image in the embedding, the correlation between the R, G, and B channels can be used in addition to the RDH algorithm of the gray image. In the development process of the color space, CIE1931RGB, CIE1960UCS and CIE1976$L^*a^*b^*$, CIEDE2000 have been developed. In the following, we describe some classical RDH methods from these two subclasses, and some applications of the CIE color space and the development history of CIE color space.

A. RDH Methods Based on Gray Image

These RDH methods based on gray image can be roughly divided into four categories of lossless compression [6]–[8], histogram shifting (HS) [9]–[12], difference expansion (DE) [13] and prediction error expansion (PEE) [14]–[16]. The main idea of lossless compression is to compress the cover medium such as the least significant bit (LSB). Fridrich *et al.* [6] proposed to decompose the gray image into the binary bit plane, and selected the bit plane with the largest redundancy for compression, and then embedded the message. However, in this approach the embedding capacity depends mainly on the lossless compression capacity, and is insufficient. Then, Tian [13] proposed a DE technique that divides an image into N pixel pairs and hides 1 bit of data with each legitimate pixel pair. Its embedding capacity can reach 0.5 bpp, but the uncompressed location map is 0.5 bpp, so that it is necessary to reduce the location map in order to improve the embedding capacity. Therefore, Hu *et al.* [17] proposed to improve the location map in order to greatly improve the embedding capacity. Affected by the DE, some researchers proposed the PEE that uses the pixel prediction mechanism and the spatial redundancy of natural images such as the minimum rate criterion prediction [16], the median edge detection [18], gradient adjusted prediction [19], interpolation prediction [20], rhombus prediction [21] and least square prediction(LS) [22] etc., to effectively implement RDH based on pixel prediction. In addition to DE, HS is also a powerful method. Ni *et al.* [9] first proposed an HS algorithm that generates a histogram based on the gray value of the image and hides the data reversibly by modifying the histogram. Then, Wang *et al.* [23] proposed a novel RDH general framework using multiple histograms modification (MH_RDH), and Chang *et al.* [24] proposed adaptive pairwise PEE (APPEE) to adaptively design the 2D mapping according to the distribution of 2D PEH.

B. RDH Methods Based on Color Image

While all of the above-mentioned methods illustrate the extensive research and development of RDH, we noticed that most of the existing research on RDH usually focuses on gray image, with relatively few methods dedicated to color images. However, the color images are also more popular than gray image for actual application, because color is a powerful visual descriptor and can simplify the recognition of the objects in the scene. The RDH method of color image adds the research on the correlation between the three channels of the color image on the basis of the gray image RDH method. To date, some of the existing color image RDH methods only used gray image RDH methods in the R, G, and B channels directly rather than considering the correlation of the three channels. Subsequently, Li *et al.* [25] proposed the use of edge information from the reference channels and inter channel correlation to improve the efficiency of the PEE and the prediction accuracy. Then, Ou *et al.* [26] utilized the inter channel correlation for payload partition and adaptive embedding to achieve minimal distortion. Recently, Yao *et al.* [27] proposed to improve the prediction performance by guided filtering based on color images, and Hou *et al.* [28] proposed a RDH scheme that maintained the same grayscale of the marked image as the cover image after embedding. However, most existing color image RDH methods do not consider the different subjective visual perception in each R, G, and B color channels, and they all use the peak signal to noise ratio (PSNR) as the criteria for the assessment of the marked images' quality. However, the PSNR metric is inconsistent with the subjective feeling of human eyes in image quality assessment research area.

C. Research on CIELAB Space

Chromaticity analysis shows that brightness, hue, and saturation are the most intuitive parameters for describing color images. However, for CIERGB [29] and CIEUCS [30], due to the subjectively of the perceived color difference in the XYZ system, the larger change in the coordinates is quite different, motivating the proposal of the uniform color space CIE$L^*a^*b^*$ [31] that reflects the idea of a uniform color space, that is, the color difference between two images in the space is basically the same as the subjectively felt color difference. Subsequently, some researchers have proposed an improved method for the evaluation of lightness, chroma, hue weighting function CIEDE2000 [32] and it has been proposed for small color difference that has characteristics consistent with the subjective vision.

In the past decades, several researchers have applied the CIELAB space with developed S-CIELAB that corresponds to human vision such as Johnson and Fairchild [33] who proposed a general overview of the functional mechanism of S-CIELAB, and compared the spatial domain and the frequency domain filtering. KAWABATA [34] first proposed that the evaluation including visible digital watermarking

(a) Marked image 1 PSNR:32.9020dB ΔE:4.2201 (b) Cover image of Airplane (c) Marked image 2 PSNR:32.9020dB ΔE:0.9578

(d) Marked image 3 PSNR:29.3802dB ΔE:8.3704 (e) Cover image of Barbara (f) Marked image 4 PSNR:29.3802dB ΔE:1.5043

Fig. 1. Comparing the results of CIEDE2000 and PSNR metrics for assessing the color image quality in "Airplane" and "Barbara" images.

should be performed on the multi-view 3D CG image quality, and then KAWABATA and MIYAO, [35] proposed to use both the S-CIELAB color space and CIEDE2000 to evaluate Multi-View 3D CG image quality for contrast enhancement, Bai *et al.* [36] proposed an effective color metric that can predict the perceptual image quality for the Retinex method based on the S-CIELAB color space. Hirai *et al.* [37] proposed SV-CIELAB which is an objective video quality assessment (VQA) method using a spatio-velocity contrast sensitivity function (SV-CSF).

III. Image Quality Assessment Metric of CIEDE2000

Currently, most of RDH methods use PSNR as a metric to assess the quality of the marked gray or color image. However, image quality assessment research had proved that the PSNR metric was inconsistent with subjective visual perception and it not suitable for the assessment of image quality. Therefore, in this section, we introduce the CIEDE2000 color image quality assessment metric that is used as the assessment metric in this paper and compare it to the PSNR for the evaluation of the visual quality.

CIEDE2000 is regarded as the best uniform color-difference model that is in agreement with the subjective visual perception and is published by the International Commission on Illumination (CIE). The specific formula of CIEDE2000 is as follows:

$$\Delta E = \sqrt{\left(\frac{\Delta L'}{K_L S_L}\right)^2 + \left(\frac{\Delta C'}{K_C S_C}\right)^2 + \left(\frac{\Delta H'}{K_H S_H}\right)^2 + R_T \left(\frac{\Delta C'}{K_C S_C}\right)^2 \left(\frac{\Delta H'}{K_H S_H}\right)^2} \tag{1}$$

where ΔE is the color difference value, $\Delta L'$ is the lightness difference, $\Delta C'$ is the chroma difference, $\Delta H'$ is the huge difference, K_L, K_C, K_H are correction factors related to the observed environment lightness, S_L, S_C, S_H describe the visual perception action on the three attributes, and R_T was used to correct the deflection in the blue region of the ellipse axis direction for visual perception. In addition, Table I shows the relationship between the CIEDE2000 color-difference parameter ΔE and subjective perception. A smaller value of the color-difference parameter ΔE implies a higher quality of agreement with the subjective perception.

TABLE I

Subjective Assessment Metric Based on CIEDE2000 Color Difference

k	$\Delta E_{\min}(k)$	$\Delta E_{\max}(k)$	Perception of color difference
1	0.0	0.5	Hardly
2	0.5	1.5	Slight
3	1.5	3.0	Noticeable
4	3.0	6.0	Appreciable
5	6.0	12.0	Much
6	12.0	24.0	Very much
7	24.0	∞	Strongly

In this work, we perform a series of experiments to compare the result of the CIEDE2000 and PSNR metrics for assessing the color image quality. We calculate the CIEDE2000 difference between the marked image and the original image as ΔE. As shown in Fig. 1, Fig. 1(b) and Fig. 1(e) are the "Airplane" image and the "Barbara" image. Fig. 1 (a) and Fig. 1(c) are marked as "Airplane" images, and Fig. 1(d) and Fig. 1(f) are marked as the "Barbara" images.According to the subjective perception, the visual differences between Fig. 1(a) and Fig. 1(b) are extremely strong, and in particular, the background color is much whiter than the original image, but the visual difference between Fig. 1(c) and Fig. 1(b) is quite small; again, the visual difference between Fig. 1(d) and Fig. 1(e) is also extremely strong, in particular, the color of the scarf, trousers and tablecloth are different from the original image,

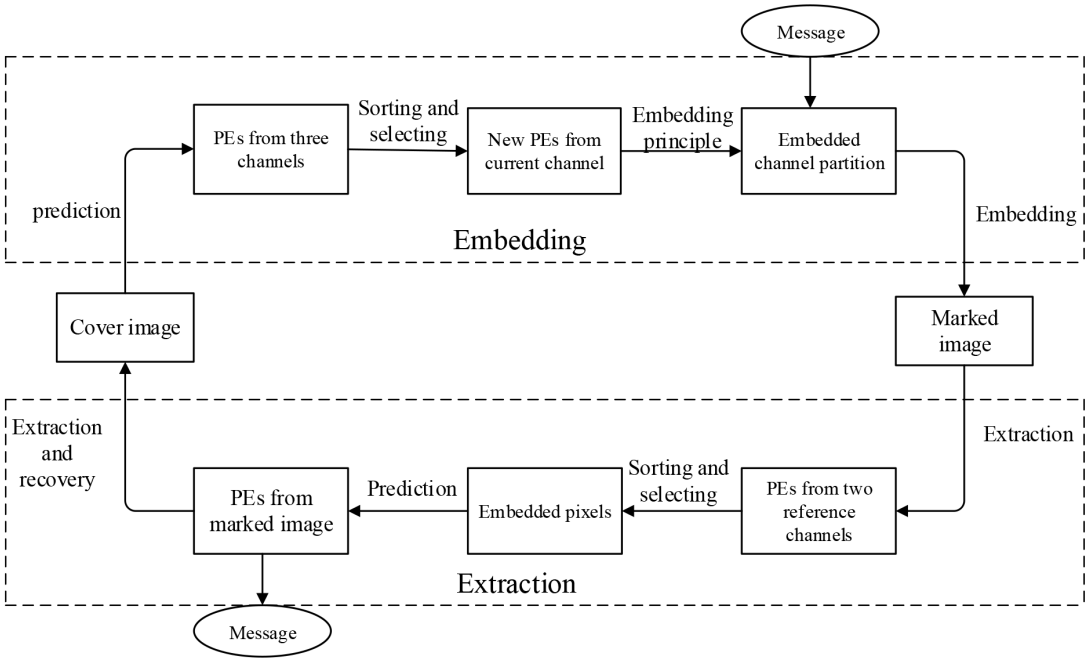

Fig. 2. Overview of the proposed algorithm.

but the visual difference between Fig. 1(c) and Fig. 1(b) is much smaller. Objectively, the CIEDE2000 values of Fig. 1(a) and Fig. 1(c) are 4.2201 and 0.9578, and the values from Fig. 1(d) and Fig. 1(f) are 8.3704 and 1.5043, respectively; all of these reflect the subjective perception correctly, but the PSNR values of Fig. 1(a) and Fig. 1(c) are both 32.9020dB, and are 29.3802dB for Fig. 1(d) and Fig. 1(f); these values are all not consistent with the subjective perception. Therefore, CIEDE2000 is more consistent for subjective perception than PSNR as an assessment metric for color images.

The PSNR results are inconsistent with the subjective perception because our method calculates the PSNR on the three channels R, G, and B, respectively, and calculates the mean of the three PSNR values to obtain the final PSNR result; this approach does not consider the different visual perception between the three channels of the color images. Therefore, we use CIEDE2000 as the assessment metric of the color images because it is regarded as the best uniform color difference model coinciding with subjective visual perception.

IV. Proposed Method

Most of the existing RDH methods take PSNR as the criteria to assess the marked image's quality, even though it has been proved that PSNR is not consistent with the subjective feeling of human vision. In this work, we propose a novel B-R-G embedding principle by applying different visual perception in each of the R, G, and B color channels. First, we predict the original image by proposing a double-layer LS prediction method. Second, we select the embedded pixels by sorting and excluding the high-energy pixels by using the energy threshold. Finally, the data are embedded into the selected pixels using the B-R-G embedding principle. The overview of the proposed algorithm as shown in Fig. 2.

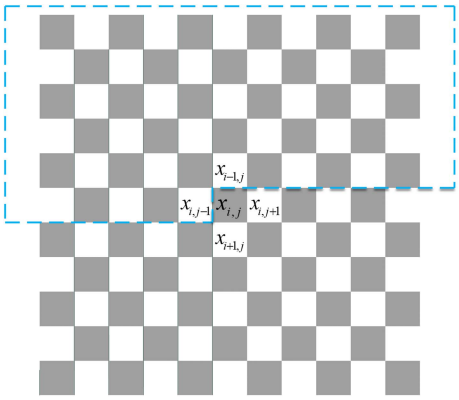

Fig. 3. Double-layer LS prediction scheme.

A. Double-Layer LS Predictor

It is well-known that rhombus prediction [21] and LS Prediction(LS) [22] are the two most widely used prediction algorithms. The wide use of the Rhombus prediction is mainly due to its relatively accurate predictions, and it can be used for sorting in some RDH methods. The advantage of the LS prediction is that it can predict more accurately by using more original pixels. However, it cannot be used for some pixels that must be sorted due to its causal order mechanism. Therefore, we propose a double-layer LS prediction by combining the characteristics of Rhombus prediction and LS prediction.

The double-layer embedding on the color image is divided into two layers, with the black pixels representing the "Dot" sets and white pixels representing the "Cross" sets. In the first stage, we process the "Cross" sets in three channels to embed a half of the payload. Then, we process the "Dot" sets in three channels to embed the other half of the payload. Since the embedding methods are same in the two layers, we use

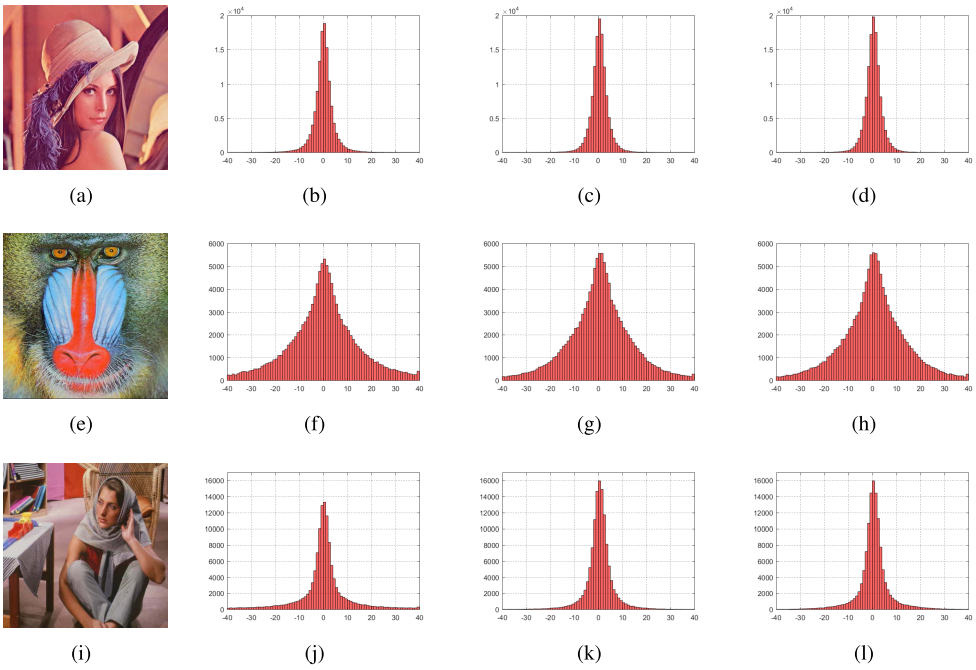

Fig. 4. Prediction error histograms on "Lena", "Baboon" and "Barbara" by using different predictors: (b),(f),(j) Rhombus predictor [21] (c),(g),(k) LS predictor [22] (d),(h),(l) Double-layer LS predictor.

the the "Cross" set as an example to introduce the prediction process in this paper.

Assume that size of the block is B*B. In this block, image pixels are estimated by a weighted sum over a certain neighborhood of $x_{i,j}$ by the prediction, for convenience, we define the indexing of the neighborhood as $x_{i,j}^1, \ldots\ldots, x_{i,j}^k$, where k is the order of the predictor. Let $\mathbf{x}$ be the row vector $\mathbf{x} = [x_{i,j}^1, \ldots\ldots, x_{i,j}^k]$ obtained by ordering the context of $x_{i,j}$ according to the indexing, and $\mathbf{v} = [v_1, \ldots\ldots, v_k]'$ as the column vector with the coefficients of the prediction. The predicted pixel can be written as:

$$\hat{x}_{i,j} = \mathbf{xv} \tag{2}$$

We remind that the LS considers the weights that minimize the sum of the squares of the prediction error. The formula is given as:

$$\min \sum_i \sum_j e_{i,j}(\mathbf{v})^2 \tag{3}$$

where $e_{i,j}$ is the prediction error of image pixel $x_{i,j}$, and v is the column vector with the coefficients of the prediction.

By taking the partial derivatives of Eq.(3) with respect to the components of v and setting them equal to zero, we finally obtain

$$v = (\mathbf{X}^T\mathbf{X})^{-1}\mathbf{X}^T\mathbf{y} \tag{4}$$

where $\mathbf{y}$ is the column vector obtained by scanning the block along the rows, and $\mathbf{X}$ is a matrix for which the rows are the vectors $(x_{i,j}^1, \ldots\ldots, x_{i,j}^k)$ of the corresponding pixels.

Then, the predicted value $\hat{x}$ is obtained by this method. To avoid the waste of the pixels around the image, we use the Rhombus prediction to calculate the prediction-error of the surrounding pixels. The prediction-error $e_{i,j}$ is given by

$$e_i = x_i - \hat{x}_i \tag{5}$$

where x_i and $\hat{x}_i$ represent the original and predicted values of the pixel, respectively. Since the color image includes the R, G, and B channels, the prediction errors in the three channels are calculated in the same manner. We obtain three prediction-error sequences using Eq.(5) as (e_1^R,……,e_N^R), (e_1^G,……,e_N^G), and (e_1^B,……,e_N^B), where N is the number of pixels involved in the prediction of each channel.

It should be mentioned that since the color image is divided into the "Cross" set and the "Dot" set, we only have the "Dot" set pixels when predicting the "Cross" set pixels, so that the "Cross" set pixels are replaced by calculating the average of the surrounding pixels as follows:

$$\widetilde{x}_{i,j} = (x_{i,j+1} + x_{i,j-1} + x_{i-1,j} + x_{i+1,j})/4 \tag{6}$$

where $\widetilde{x}_{i,j}$ is the replaced pixel, $x_{i,j-1}$,$x_{i,j+1}$, $x_{i-1,j}$, $x_{i+1,j}$ represent the neighborhood of $x_{i,j}$, and the pixels in the edge of the block are used to help replace the pixels of the "Cross" set. Thus, we obtain a new block to predict.

To represent the performance of the double-layer LS prediction, we predict the pixels in the "Cross" set of R channel in "Lena", "Baboon", and "Barbara" images by using Rhombus prediction, LS prediction and Double-layer LS prediction. The results are shown in Fig. 4. It is observed that the Double-layer LS prediction displays a better performance than the Rhombus prediction and is as good as the LS prediction. In addition, the Double-layer LS prediction can satisfy some RDH algorithms that need to be sorted.

B. Selection of Embedding Pixels

Generally, the prediction result is often more accurate in the smooth region because the pixel values in the smooth region are mostly similar. Hence, to reduce the embedding distortion, we first select the smooth region in the image to

TABLE II
PERFORMANCE COMPARISON OF ΔE VALUES WITH THE DIFFERENT ΔD_T

Embedding Capacity(bits)	ΔD_T=0.05	ΔD_T=0.5	ΔD_T=1	ΔD_T=1.5	ΔD_T=2
100000	0.0735	0.0737	0.074	0.0744	0.0747
110000	0.0823	0.0823	0.0835	0.0843	0.0862
120000	0.0911	0.0911	0.0920	0.0926	0.0938
130000	0.0990	0.0990	0.1005	0.1014	0.1022
140000	0.1037	0.1037	0.1043	0.1058	0.1091
150000	0.1088	0.1089	0.1093	0.1123	0.1143
160000	0.1136	0.1138	0.1145	0.1174	0.1208
170000	0.1186	0.1187	0.1194	0.1242	0.1287
180000	0.1233	0.1237	0.1256	0.1312	0.1336
190000	0.1285	0.1287	0.1303	0.1353	0.1379
200000	0.1334	0.1338	0.1358	0.1423	0.1449

embed the secret data. Here, the proposed method sorts the pixels according to the local variance Ω_i to calculate the complexity. The complexity of each central pixel $x_{i,j}'s$ can be computed from the neighboring pixels $x_{i,j-1}$, $x_{i,j+1}$, $x_{i-1,j}$ and $x_{i+1,j}$ (as shown in Fig. 3) as follows:

$$\Omega_i = \frac{1}{4}\sum_{k=1}^{4}(\Delta v_k - \Delta\overline{v})^2 \tag{7}$$

where Δv_k is the absolute value of the difference between the neighborhood of the certain pixel $x_{i,j}$, details as follows: $\Delta v_1 = |x_{i,j-1} - x_{i-1,j}|$, $\Delta v_2 = |x_{i-1,j} - x_{i,j+1}|$, $\Delta v_3 = |x_{i,j+1} - x_{i+1,j}|$ and $\Delta v_4 = |x_{i+1,j} - x_{i,j-1}|$, $\Delta\overline{v}$ is average of the Δv_k, $\Delta\overline{v} = (\Delta v_1 + \Delta v_2 + \Delta v_3 + \Delta v_4)/4$. Local variance Ω_i is calculated by using Eq.(7) to achieve the appropriate sorting for improving performance of data hiding.

Because the color images include the R, G, and B channels, the complexities in the three channels are calculated in the same manner. If the current channel's complexity is denoted as Ω_i^c, the other two reference channels' complexities are denoted as Ω_i^{r1} and Ω_i^{r2}, respectively. To consider the correlation of the three channels, the more effective color complexity Ω_i^L is given as

$$\Omega_i^L = 1.5\Omega_i^c + \Omega_i^{r1} + \Omega_i^{r2} \tag{8}$$

Here, the current channel's complexity Ω_i^c is assigned a larger weight, because the correlation of the current channel is more important than the other two reference channels' complexities. Then, the original prediction-error sequence is sorted in the ascending order of Ω_i^L and three new prediction error sequences are obtained as $(e^B_{\sigma 1}, \ldots\ldots, e^B_{\sigma N})$,$(e^R_{\sigma 1}, \ldots\ldots, e^R_{\sigma N})$, and $(e^G_{\sigma 1}, \ldots\ldots, e^G_{\sigma N})$, where σ is the unique one-to-one mapping.

Currently, the total distortion in most of the existing RDH methods often consists of the embedding distortion and the shifting distortion. To reduce the total distortion caused by the embedding process, the proposed method embeds the message one by one into the prediction error sequence that can avoid the shifting distortion. However, there are some pixels with large prediction error that will cause a larger distortion in the embedding process. Hence, the prediction errors in the other two reference channels are used to exclude the high-energy prediction error because the R, G, and B channels in color images are strongly correlated. That is, the prediction error with its references below an energy threshold is selected for embedding. The prediction error sequences $(e_1^{r1},\ldots\ldots,e_N^{r1})$, $(e_1^{r2},\ldots\ldots,e_N^{r2})$ represent two reference prediction errors of the reference channels, $(e_1,\ldots\ldots,e_N)$ represents a prediction error of the current channel. We define the energy threshold as D_T to select the pixels for embedding. Here, we initialize D_T as 0, and each time increase the value of D_T by 0.5 until the selected pixels can meet the embedding requirements. The specific formula is:

$$D_i = \sqrt{(e_i^{r1})^2 + (e_i^{r2})^2} \tag{9}$$

where e_i^{r1} and e_i^{r2} represent the prediction errors of the two reference channels at the same pixel.D_i represents the energy threshold of the current channel. If $D_i > D_T$, we define this pixel as a high-energy pixel and exclude it from the above prediction error sequence, and obtain new prediction error sequence pixels $(e_{\sigma 1}, \ldots\ldots, e_{\sigma M})$, where $M <= N$.

In order to explain why increase the value of D_T by 0.5 for each time, we define the incremental energy threshold as ΔD_T. We take the "Barbara" image as an example to indicate the influence of value by the ΔD_T as 0.05, 0.5, 1, 1.5 and 2 respectively in different embedding capacity. It should be mentioned that smaller ΔE values, corresponds to higher performance. As shown in table II, with the increase of the ΔD_T, ΔE values are increased. Hence, the smaller the ΔD_T, the better the results. However, considering the time complexity, if ΔD_T is 0.05, it will take 10 times longer than in 0.5. Therefore, we comprehensively to choose ΔD_T increasing by 0.5 each time.

To illustrate the requirement to exclude the high-energy pixel in the proposed method, we perform an experiment to prove that using D_T can reduce the total modifications. We compare the total embedding modifications obtained with and without the use of D_T. This is described by:

$$T_m = \sum_{x=0}^{M}\sum_{y=0}^{N}|I'_{(x,y)} - I_{(x,y)}| \tag{10}$$

where T_m represents the total modifications, I' represents the marked image, and I represents the original image.

As shown in Fig. 5, we use the threshold D_T to obtain smaller modifications compared to the modification obtained without the use of D_T. This is because we use D_T to exclude

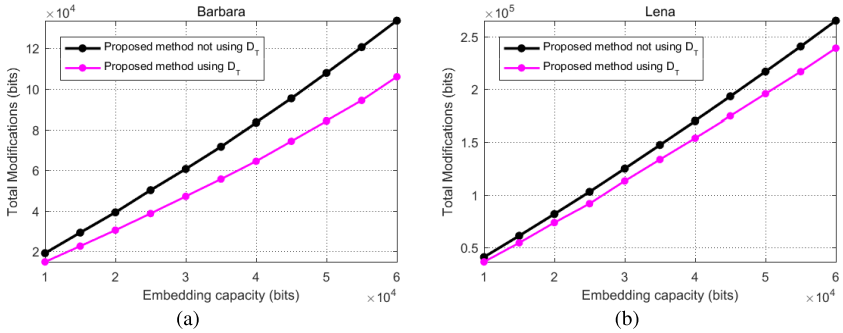

Fig. 5. The total modifications of "Barbara" and "Lena", respectively.

the high energy pixels; in other words, we can use the energy threshold to select the pixels and embed the message into the low-energy values' pixels to reduce the embedding distortion. Thus, the threshold D_T is more useful to our performance in later experiments.

C. B-R-G Embedding Principle

Currently, most of the RDH methods use PSNR as the assessment metric to assess the quality of marked grayscale or color images. However, image quality assessment research has proved that the PSNR metric is inconsistent with subjective visual perception and is not suitable for the assessment of image quality. In fact, it has been proven that the R, G, B channels of the color image have different visual perception to human eyes by the brightness conversion formula as:

$$Y = 0.299 * R + 0.114 * B + 0.587 * G \tag{11}$$

where Y represents the converted brightness value, R, G, and B represent the pixel of three channels at the same coordinate.

The brightness conversion formula in Eq.(11) shows that the G channel has the greatest weight, followed by the R channel, and the weight of B channel is the lowest. This means that when we embed more secret bits in the B channel, the impact on human vision is smaller than that obtained by embedding the same number of secret bits in the R and G channels; it also shows that the G channel has the greatest influence on the visual perception of human eyes.

Therefore, inspired by the brightness conversion formula, we propose the B-R-G embedding principle that is more suitable for color images. This B-R-G embedding principle embeds the secret data into the B channel first, then embeds the secret data into the R channel, and then embeds the secret data into the G channel. The embedding process is shown in Fig. 6. It should be mentioned that in order to maintain the correlation between each R, G, and B channels, the proposed method modifies as few of the pixels as possible, so that only one half of the total set of the pixels are used for embedding in order to obtained greatly improved prediction performance in the other pixels. Thus, we can ensure that the method is still effective for embedding the second layer of each channel under large embedding capacity. The specific steps are as follows: first, the secret message is divided into two halves and the two halves are embedded into B_1 and B_2, respectively. Second, if the maximum embedding capacity

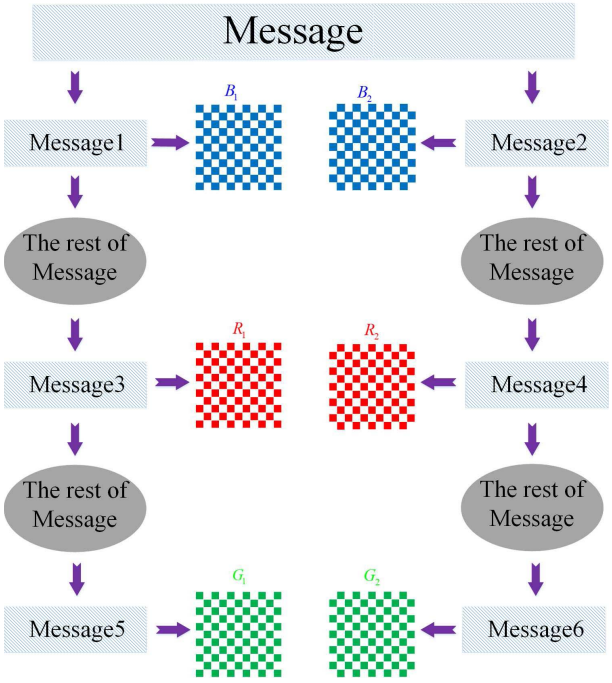

Fig. 6. Diagram of the proposed embedding method for color images.

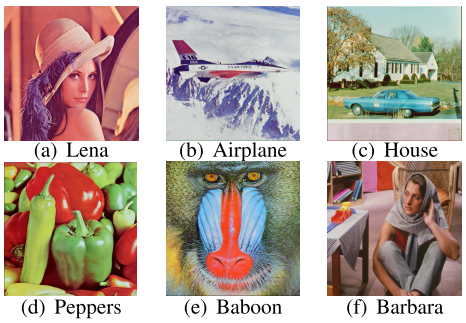

Fig. 7. Six test cover images.

of the B channel is not sufficient for embedding the entire secret message, the remaining secret message is divided into halves and the two halves are embedded into R_1 and R_2, respectively. Last, if the maximum embedding capacity of the R channel is not sufficient to embed the remaining secret message, the remaining secret message is divided into halves and the two halves are embedded into G_1 and G_2, respectively. It should be mentioned that the maximum embedding capacity

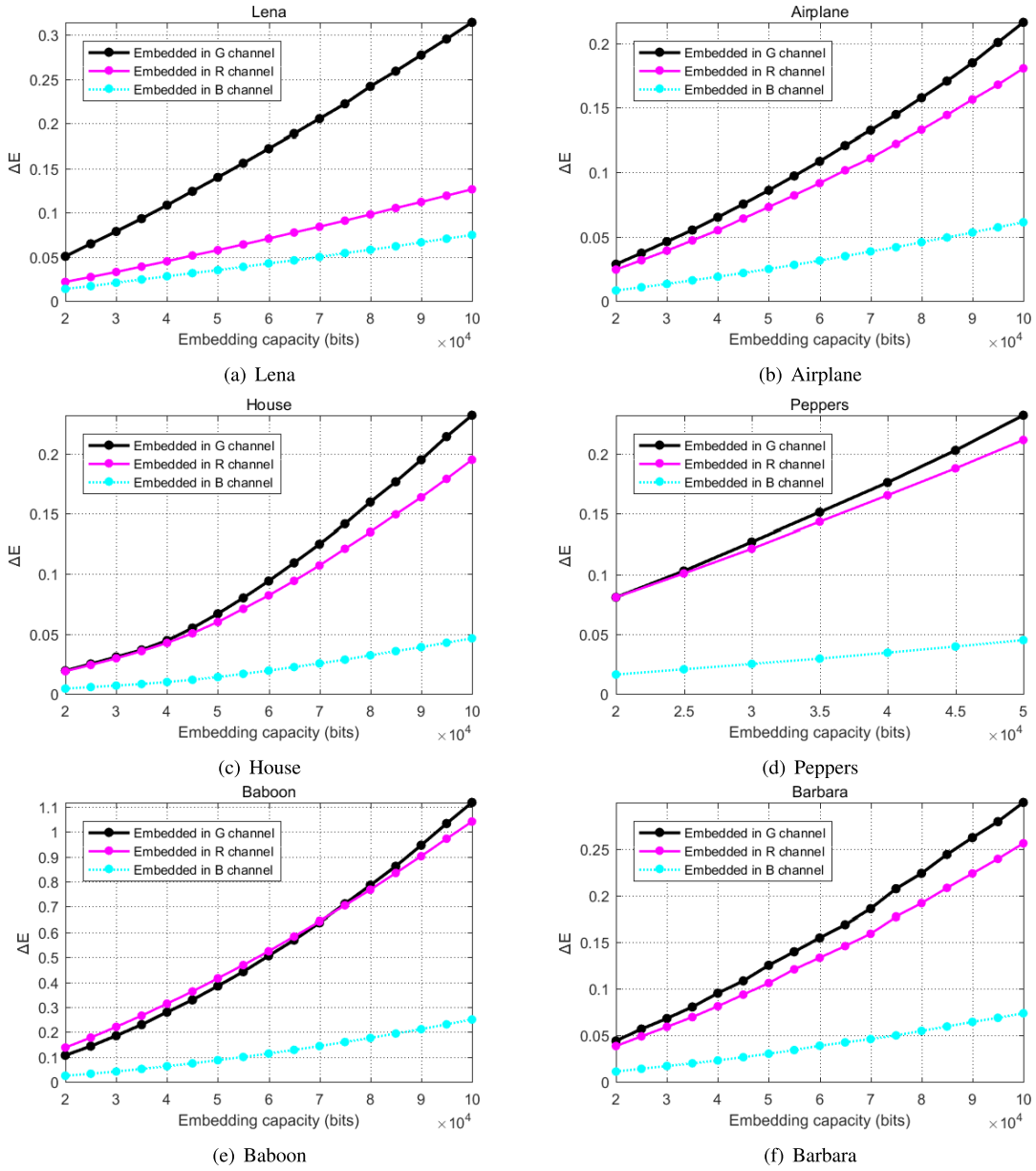

Fig. 8. Performance comparison of ΔE values between R, G, B channels of six color images.

in each channel is determined as one half of the total number of the pixels in this channel.

D. Embedding Procedure

In this section, we will introduce the embedding procedure. Because the embedded methods in three channels are identical, we use the "Cross" set in the B channel as an example.

1. Predict the "Cross" set pixels of B, R, G channels through double-layer LS prediction and obtain the prediction errors sequence(e_1^R,……,e_N^R), (e_1^G,……,e_N^G), and (e_1^B,……,e_N^B). The details of the calculation are described in section IV-A, and we obtain $\hat{x}_{i,j}$ from Eq.(2), $e_{i,j}$ from Eq.(5).

2. Sort the prediction error of the B, R, and G channels as $(e^B_{\sigma 1}, \ldots\ldots, e^B_{\sigma N})$,$(e^R_{\sigma 1}, \ldots\ldots, e^R_{\sigma N})$, and $(e^G_{\sigma 1}, \ldots\ldots, e^G_{\sigma N})$, select the embeddable prediction errors by the energy threshold D_T and obtain a new prediction error sequence $(e^B_{\sigma 1}, \ldots\ldots, e^B_{\sigma M})$. The calculation details are provided in section IV-B.

3. Embed data into the pixels in the corresponding embeddable prediction-error sequence. The marked pixels are calculated as

$$x' = \hat{x} + 2 * e + b \tag{12}$$

where x' represents the marked pixel, $\hat{x}$ is the predicted value and the e is the prediction error of x, $b \in (0, 1)$ is the secret data to be embedded. The calculation details are provided in section IV-C.

In the embedding process, if an overflow occurs, it will be recorded as 1 on the location map, and the rest will be recorded as 0. The location maps are compressed losslessly by Arithmetic coding simulation [38]. For the blind extraction, the auxiliary information includes: the length of the compressed location maps in the three channels as (L^R,L^G,L^B),

payload partition in the three channels as (EC_R,EC_B,EC_G), the energy thresholds in the three channels as (D_T^R, D_T^G, D_T^B), and the compressed location maps in the three channels as (Loc^R, Loc^G, Loc^B). All auxiliary information is replaced in the LSB_s of the four sides of the three channels respectively. The original LSB stream is embedded into the images as a part of the secret message.

E. Extracting Procedure

Sections IV-D illustrates the data embedding procedure. In the order opposite to the embedding order, we first carry out extraction and recovery processing in the G channel, and the message extraction is in the order of G-R-B. Because the extraction methods for the three channels are the same, we use the "Dot" set in the G channel as an example. The detailed procedure for data extraction and recovery is described as follows:

1. Read LSB of the four sides in the G channel and obtain the auxiliary information of the G channel including the length of the compressed location maps in the three channels as L^G, the payload partition in the three channels as EC_G, the energy thresholds in the G channels as D_T^G, and the compressed location maps in the G channel as Loc_G.

2. Predict the pixels of the B and R channels through double-layer LS prediction, obtain the prediction-error (e_1^R,……,e_N^R), (e_1^B,……,e_N^B). The calculation details are provided in section IV-A.

3. Calculate the complexity Ω_i^L and sort the prediction-error sequence (e_1^R,……,e_N^R), (e_1^B,……,e_N^B) in the ascending order. Then, obtain the embedded pixels through the extracted values of D_T, the payload of G channel EC_G and the compressed location maps Loc_G. The calculation details are provided in section IV-B and IV-C.

4. Predict those modified pixels in order from bottom to top, right to left by using the double-layer LS prediction in the G channel to obtain expand prediction error sequence e_i', an then extract the secret data repeatedly according to

$$\begin{cases} b = e' \bmod 2 \\ e = \lfloor e'/2 \rfloor \end{cases} \tag{13}$$

where $\lfloor x \rfloor$ returns the nearest integer less than or equal to x, e is the original prediction error.

5. Recover the pixels according to:

$$x = x' - e \tag{14}$$

where x' represents the marked pixel, x is the original pixel and the e is the prediction error of x.

6. Replace the LSBs of the four sides in the G channel, and recover all of the original image.

The extractions of the R and B channels are the same as that of the G channel. When the extractions for the three channels are completed and the secret image is restored, all of the extractions and restorations are completed.

V. Experimental Results

This section presents experiments and results of the proposed method. The experiments are tested in Windows 10 by Matlab 2016 and with Inter(R) Core(TM) i7 2.60 GHz CPU and 8.0 GB RAM. Six standard cover images are shown in Fig. 7, in which five standard 512*512 sized color images from USC-SIPI database [39], including "Lena", "Airplane", "House", "Baboon", "Peppers" and one standard 510*510 sized color image "Barbara" is from LIVE database [40]. To evaluate the proposed method more objectively, the performance of the proposed method was compared to the performance of the methods developed by Ou *et al.* [26], Hou *et al.* [28] and Yao *et al.* [27] that are the current state-of-the-art color image RDH methods, and to the method developed by Hu *et al.* [16] that is an RDH method based on the gray image with optimal performance.

TABLE III

Performance Comparison of ΔE Values Between the Proposed Method and Ordinary Equal Partition Scheme on Six Standard Images

Image (capacity(bits))	Equal partition scheme	Proposed scheme
Lena(30000))	0.044	**0.021**
Baboon(30000)	0.157	**0.043**
Airplane(30000)	0.028	**0.013**
Barbara(30000)	0.047	**0.017**
House(30000)	0.020	**0.007**
Peppers(30000)	0.115	**0.025**
Lena(60000)	0.091	**0.042**
Baboon(60000)	0.360	**0.120**
Airplane(60000)	0.057	**0.031**
Barbara(60000)	0.098	**0.038**
House(60000)	0.035	**0.020**
Peppers(60000)	0.237	**0.055**
Average	0.107	**0.036**

As mentioned above, we propose the B-R-G embedding principle to embed the data in the B channel, the R channel and the G channel order, and use the CIEDE2000 metric to assess the visual quality of the marked images. To prove the effectiveness of the B-R-G embedding principle and the consistency between the CIEDE2000 metric and subjective visual perception, we embed identical messages into the B, R, and G channels of the six standard color images respectively. As shown in Fig. 8, the results obtained using CIEDE2000 are different in the three channels after embedding the same messages, and the ΔE values in the B channels are the smallest, followed by ΔE values of the R channels, and the largest ΔE values are obtained for the G channels. This reflects the fact that when we embed the message into the B channels, the impact on human vision is smaller than for the embedding of the same number of messages into the R and G channels, and also shows that the G channel has the greatest influence on the visual perception of human eyes. These results also proved that the R, G, and B channels of the color images have different visual perception to human eyes in the brightness conversion formula.

In addition, we propose the B-R-G embedding principle to embed the data sequential in the B, R and G channels, and the maximum embedding capacity in each channels is determined by the half of the total number of the pixels in this channel. Therefore, to demonstrate the efficiency of the proposed methods, the ΔE comparisons between the ordinary

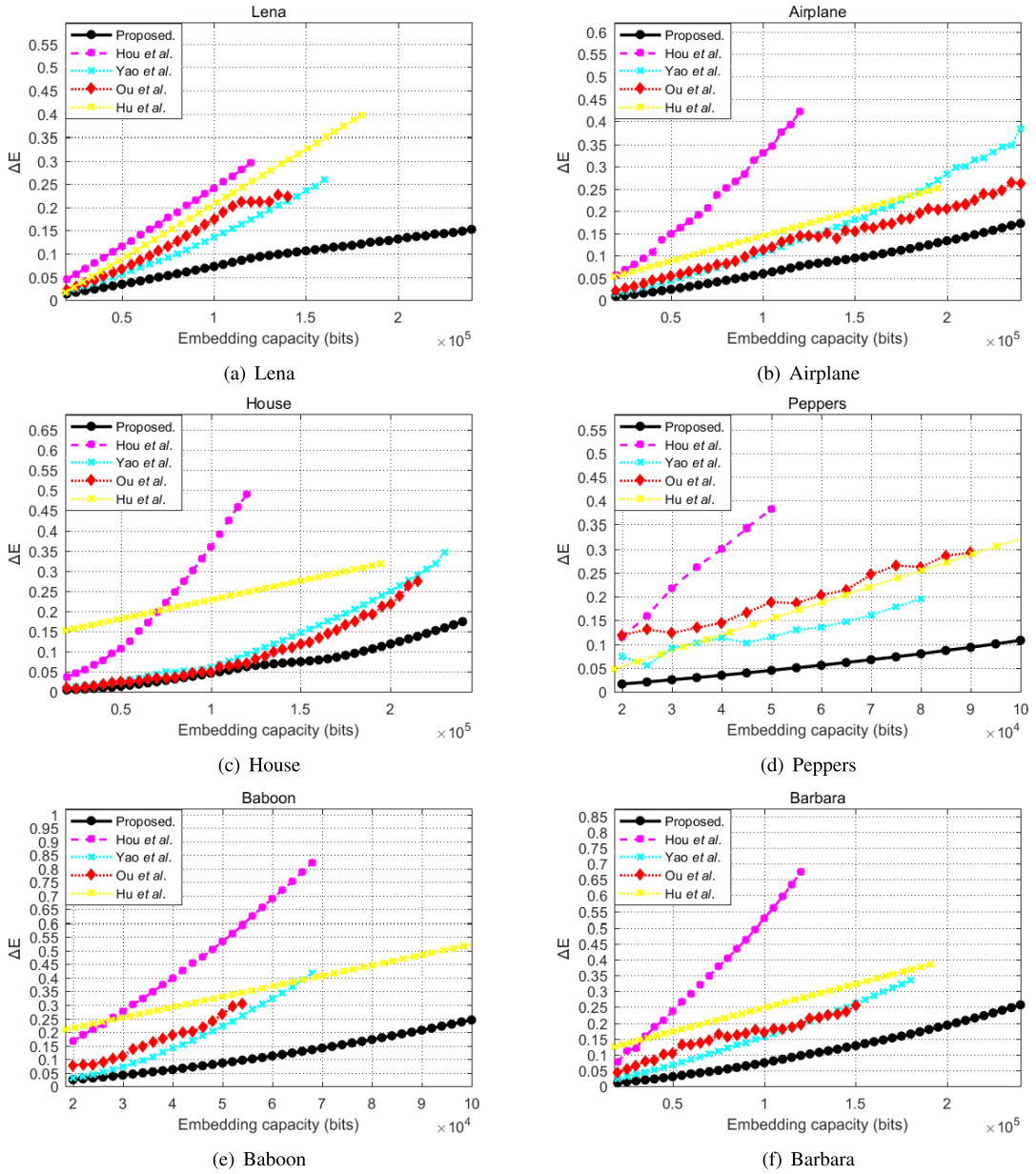

(a) Lena (b) Airplane

(c) House (d) Peppers

(e) Baboon (f) Barbara

Fig. 9. Performance comparison between proposed method and other four methods of Ou *et al.* [26], Hou *et al.* [28], Yao *et al.* [27], Hu *et al.* [16].

TABLE IV

PERFORMANCE COMPARISON OF ΔE VALUES BETWEEN THE PROPOSED METHOD AND FOUR OTHER RDH METHODS FOR SIX STANDARD IMAGES WHEN EMBEDDING CAPACITY IS 50000BITS, RESPECTIVELY. THE BEST RESULT FOR EACH IMAGE IS SHOWN BY BOLDFACE

Image	Ou *et al.* [26].	Yao *et al.* [27].	Hou *et al.* [28].	Hu *et al.* [16].	Proposed
Lena	0.067	0.056	0.116	0.087	**0.034**
Baboon	0.241	0.225	0.505	0.331	**0.086**
Airplane	0.052	0.045	0.149	0.091	**0.024**
Barbara	0.104	0.068	0.237	0.173	**0.030**
House	0.025	0.026	0.108	0.184	**0.014**
Peppers	0.190	0.113	0.382	0.155	**0.045**
Average	0.113	0.089	0.250	0.170	**0.039**

equal payload allocation scheme and the proposed scheme for the six standard color images with the capacities of 30,000 and 60,000 bits are listed in Table III. An examination of the results presented in Table III shows that all of the ΔE values partitioned by the proposed methods are clearly smaller than their corresponding values obtained by the equal partition scheme. Thus, the average ΔE of the proposed scheme is 0.036, which is 0.071 less than that of the equal partition scheme. This proves the effectiviness of the B-R-G embedding principle.

TABLE V

PERFORMANCE COMPARISON OF ΔE VALUES BETWEEN THE PROPOSED METHOD AND FOUR OTHER RDH METHODS FOR SIX STANDARD IMAGES WHEN EMBEDDING CAPACITY IS 100000BITS, RESPECTIVELY. THE BEST RESULT FOR EACH IMAGE IS INDICATED IN BOLD AND "/"STANDS FOR UNAVAILABLE IN THE REQUIRED CAPACITY

Image	Ou *et al.* [26].	Yao *et al.* [27].	Hou *et al.* [28].	Hu *et al.* [16].	Proposed
Lena	0.177	0.136	0.241	0.208	**0.073**
Baboon	/	/	1.483	0.525	**0.245**
Airplane	0.113	0.105	0.330	0.145	**0.059**
Barbara	0.171	0.155	0.528	0.247	**0.074**
House	0.050	0.061	0.360	0.227	**0.046**
Peppers	/	/	0.869	0.323	**0.108**
Average	0.128	0.114	0.365	0.207	**0.063**

TABLE VI

PERFORMANCE COMPARISON OF EMBEDDING CAPACITY BETWEEN THE PROPOSED METHOD AND FOUR OTHER RDH METHODS FOR SIX STANDARD IMAGES WHEN ΔE IS 0.2, RESPECTIVELY. THE BEST RESULT FOR EACH IMAGE IS SHOWN BY BOLDFACE

Image	Ou *et al.* [26].	Yao *et al.* [27].	Hou *et al.* [28].	Hu *et al.* [16].	Proposed
Lena	109800	133600	84200	97200	**262300**
Baboon	42900	47800	25700	18100	**88700**
Airplane	186000	163800	68700	149600	**253800**
Barbara	123200	122800	43300	68600	**204700**
House	182200	173500	71100	69600	**259800**
Peppers	59700	80100	28700	64300	**143900**

TABLE VII

PERFORMANCE COMPARISON OF EMBEDDING CAPACITY BETWEEN THE PROPOSED METHOD AND FOUR OTHER RDH METHODS FOR SIX STANDARD IMAGES WHEN ΔE IS 0.3, RESPECTIVELY. THE BEST RESULT FOR EACH IMAGE IS INDICATED IN BOLD AND "/"STANDS FOR UNAVAILABLE IN THE REQUIRED ΔE

Image	Ou *et al.* [26].	Yao *et al.* [27].	Hou *et al.* [28].	Hu *et al.* [16].	Proposed
Lena	/	/	121700	139800	**300300**
Baboon	52900	57700	31600	42300	**116100**
Airplane	/	210200	92300	/	**260300**
Barbara	/	166200	62900	135400	**256700**
House	/	218900	88600	174900	**262100**
Peppers	90100	/	39900	94500	**179300**

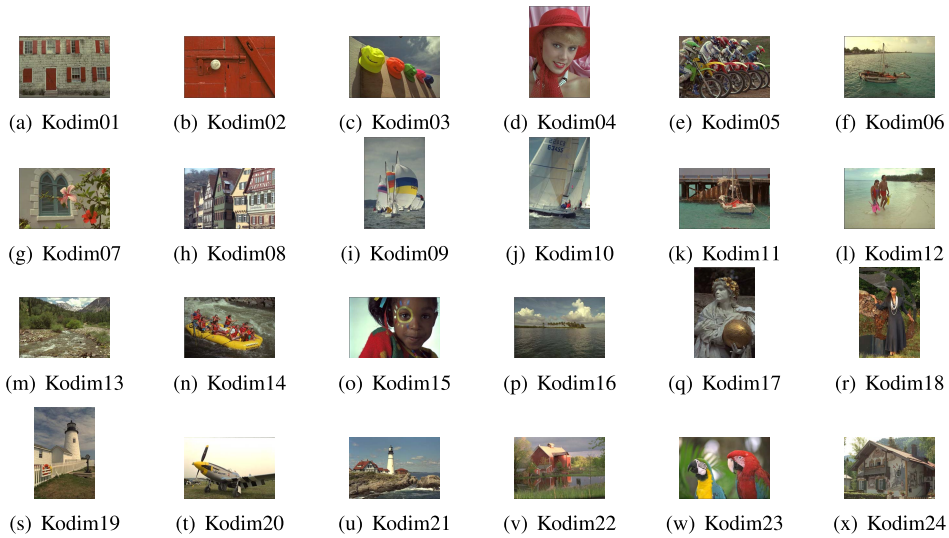

(a) Kodim01 (b) Kodim02 (c) Kodim03 (d) Kodim04 (e) Kodim05 (f) Kodim06

(g) Kodim07 (h) Kodim08 (i) Kodim09 (j) Kodim10 (k) Kodim11 (l) Kodim12

(m) Kodim13 (n) Kodim14 (o) Kodim15 (p) Kodim16 (q) Kodim17 (r) Kodim18

(s) Kodim19 (t) Kodim20 (u) Kodim21 (v) Kodim22 (w) Kodim23 (x) Kodim24

Fig. 10. Cover images from Kodak image dataset [41].

Fig. 9 shows the performance comparison of the proposed method and the methods developed by Ou *et al.* [26], Hou *et al.* [28], Yao *et al.* [27] and Hu *et al.* [16] with respect to the ΔE values. Among these methods, because the method developed by Hu *et al.* [16] is suitable for gray images, to apply it to the color image, we divide the embedding amount equally into three parts and embed them into the R, G and B channels. It is observed that the proposed method performs better than the other methods on the six images, with almost all of the ΔE values obtained by our methods smaller than the ΔE of the methods in the literature for any available capacity. It should be mentioned that smaller

TABLE VIII

PERFORMANCE COMPARISON OF ΔE VALUES BETWEEN THE PROPOSED METHOD AND FOUR OTHER RDH METHODS FOR KODAK IMAGE DATASET [41] WHEN EMBEDDING CAPACITY IS 50000BITS, RESPECTIVELY. THE BEST RESULT FOR EACH IMAGE IS INDICATED IN BOLD AND "/"STANDS FOR UNAVAILABLE IN THE REQUIRED CAPACITY

Image	Ou *et al.* [26].	Yao *et al.* [27].	Hou *et al.* [28].	Hu *et al.* [16].	Proposed
Kodim01	0.036	0.038	0.115	0.185	**0.014**
Kodim02	0.021	0.026	0.073	0.065	**0.007**
Kodim03	0.033	0.038	0.127	0.154	**0.014**
Kodim04	0.031	0.031	0.089	0.087	**0.010**
Kodim05	0.070	0.051	0.197	0.133	**0.022**
Kodim06	0.034	0.042	0.647	0.090	**0.015**
Kodim07	0.030	0.037	0.110	0.133	**0.014**
Kodim08	0.076	0.048	0.384	0.179	**0.026**
Kodim09	0.042	0.033	0.128	0.117	**0.015**
Kodim10	0.047	0.034	0.169	0.122	**0.017**
Kodim11	0.043	0.052	0.117	0.100	**0.018**
Kodim12	0.038	0.036	0.142	0.107	**0.012**
Kodim13	0.070	0.050	0.561	0.211	**0.028**
Kodim14	0.076	0.047	0.227	0.255	**0.029**
Kodim15	0.074	0.042	0.234	0.139	**0.017**
Kodim16	0.032	0.038	0.109	0.092	**0.015**
Kodim17	0.099	0.050	0.310	0.167	**0.030**
Kodim18	0.100	0.051	0.336	0.285	**0.034**
Kodim19	0.060	0.032	0.157	0.193	**0.019**
Kodim20	0.091	0.204	/	0.119	**0.052**
Kodim21	0.043	0.032	0.118	0.081	**0.016**
Kodim22	0.054	0.033	0.142	0.083	**0.017**
Kodim23	0.039	0.033	0.142	0.099	**0.016**
Kodim24	0.030	0.054	0.422	0.097	**0.023**
Average	0.051	0.040	0.220	0.138	**0.019**

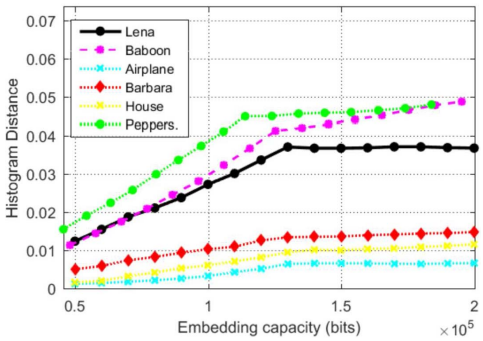

Fig. 11. The histogram distance between original image and marked image of six standard images.

ΔE values corresponds to higher performance. The higher performance of our method is mainly because our method consider the different visual perception of the R, G, and B channels of the color image, and adopts the B-R-G embedding principle to divide the embedding capacity of the R, G, and B channels, and fully exploits the visual characteristics of the color image. In addition, Fig. 9 shows that the results obtained using the methods developed by Ou *et al.* [26] and Yao *et al.* [27] do not change in a stable manner, which is due to the use of adaptive division of embedding capacity in the R, G, and B channels by these methods in order to pursue less distortion and thus achieve higher PSNR, and the consequent neglect of the different visual perception of the three channels.

For compare the performance of the proposed method and the methods developed by Ou *et al.* [26], Hou *et al.* [28], Yao *et al.* [27] and Hu *et al.* [16] with respect to the CIEDE2000 values more clearly, we provide several tables for the same embedding capacity, such as Table IV and Table V. Two different embedding capacities are selected, namely 50000 bits and 100000 bits, and the corresponding average ΔE results are shown in the tables. An examination of the results presented in these data tables shows that the average ΔE of the proposed method is better than those obtained by the other methods. Table IV indicates that the average ΔE values of all six images with the capacity of 50000 bits obtained by the Ou *et al.* [26], Yao *et al.* [27], Hou *et al.* [28], Hu *et al.*'s [16] methods and the proposed method are 0.113, 0.089, 0.250, 0.170 and 0.039, respectively. Table V indicates that the average ΔE of all six images with the capacity of 100000 bits obtained by the methods of Ou *et al.* [26], Yao *et al.* [27], Hou *et al.* [28] and Hu *et al.* [16] and the proposed method are 0.128, 0.114, 0.365, 0.207 and 0.063, respectively. Compared with other methods, the proposed method achieves average gains in the ΔE values of 0.074, 0.050, 0.211, and 0.131, respectively, for the capacity of 50000 bits, and achieves average gains in the ΔE values of 0.065, 0.051, 0.302, and 0.144, respectively for the capacity of 100000 bits. In particular, for "Baboon" and "Peppers", it is clearly from the data presented in Table V that when EC is 100000 bits, the methods of Ou *et al.* [26], Yao *et al.* [27] cannot reach this embedding capacity, while this capacity can be reached by the proposed method. This because the methods of Ou *et al.* [26] and Yao *et al.* [27] only select pixels with two fixed prediction errors to embed the data, which cannot achieve the embedding capacity.

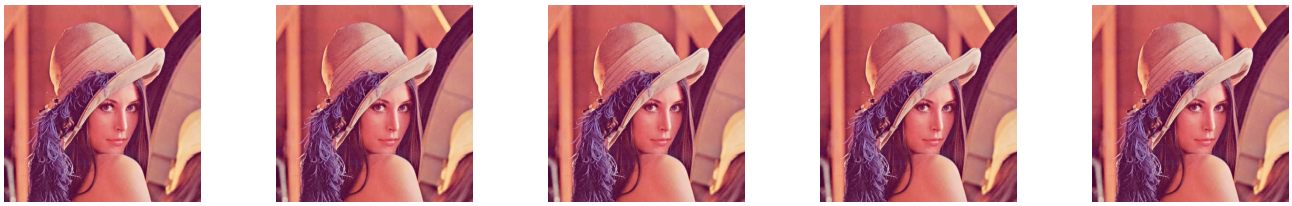

(a1)MOS: 5 ΔE:0.067 Ou *et al.* [26].
(b1)MOS: 5 ΔE:0.056 Yao *et al.* [27].
(c1)MOS: 5 ΔE:0.116 Hou *et al.* [28].
(d1)MOS: 5 ΔE:0.087 Hu *et al.* [16].
(e1)MOS: 5 ΔE:0.034 The proposed method

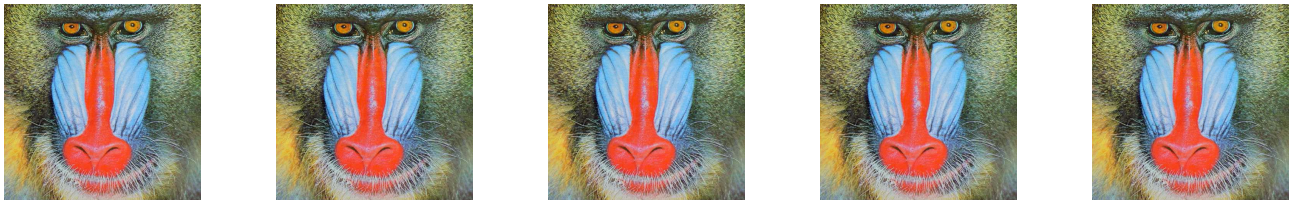

(a2)MOS: 5 ΔE:0.241 Ou *et al.* [26].
(b2)MOS: 5 ΔE:0.225 Yao *et al.* [27].
(c2)MOS: 5 ΔE:0.505 Hou *et al.* [28].
(d2)MOS: 5 ΔE:0.331 Hu *et al.* [16].
(e2)MOS: 5 ΔE:0.086 The proposed method

(a3)MOS: 5 ΔE:0.052 Ou *et al.* [26].
(b3)MOS: 5 ΔE:0.045 Yao *et al.* [27].
(c3)MOS: 5 ΔE:0.149 Hou *et al.* [28].
(d3)MOS: 5 ΔE:0.091 Hu *et al.* [16].
(e3)MOS: 5 ΔE:0.024 The proposed method

(a4)MOS: 5 ΔE:0.104 Ou *et al.* [26].
(b4)MOS: 5 ΔE:0.068 Yao *et al.* [27].
(c4)MOS: 5 ΔE:0.237 Hou *et al.* [28].
(d4)MOS: 5 ΔE:0.173 Hu *et al.* [16].
(e4)MOS: 5 ΔE:0.030 The proposed method

(a5)MOS: 5 ΔE:0.025 Ou *et al.* [26].
(b5)MOS: 5 ΔE:0.026 Yao *et al.* [27].
(c5)MOS: 5 ΔE:0.108 Hou *et al.* [28].
(d5)MOS: 5 ΔE:0.184 Hu *et al.* [16].
(e5)MOS: 5 ΔE:0.014 The proposed method

(a6)MOS: 5 ΔE:0.190 Ou *et al.* [26].
(b6)MOS: 5 ΔE:0.113 Yao *et al.* [27].
(c6)MOS: 5 ΔE:0.382 Hou *et al.* [28].
(d6)MOS: 5 ΔE:0.155 Hu *et al.* [16].
(e6)MOS: 5 ΔE:0.045 The proposed method

Fig. 12. Performance comparison of MOS values between the proposed method and four other RDH methods for six standard images when embedding capacity is 50000bits, respectively.

In order to compare the embedding capacity performance between the proposed method and other color image RDH methods, we do two experiments to show the embedding capacity in all methods on six standard images when ΔE is

0.2 and 0.3 respectively. Table VI and Table VII list that the embedding capacity between the Ou *et al.* [26], Yao *et al.* [27], Hou *et al.* [28], Hu *et al.*'s [16] methods and the proposed method on six images when ΔE is 0.2 and 0.3 respectively. It is observed that the embedding capacity of the proposed method is higher than the other four RDH methods at the same ΔE.

To further demonstrate the superiority of the proposed method, 24 color images from a Kodak image database [41] as shown in Fig. 10 are selected as the cover images for performance comparisons; here, all of the images have the dimensions of 512 *768 or 768 * 512. For a fixed embedding capacity of 50000 bits, Table VIII lists the comparison of the ΔE values obtained by the proposed method and the methods of Ou *et al.* [26], Yao *et al.* [27], Hou *et al.* [28], Hu *et al.*'s [16]. And it indicates that the average ΔE values of all 24 color images with the capacity of 50000 bits obtained by the Ou *et al.* [26], Yao *et al.* [27], Hou *et al.* [28], Hu *et al.*'s [16] methods and the proposed method are 0.051, 0.040, 0.220, 0.138 and 0.019. Compared with other methods, the proposed method achieves average gains in the ΔE values of 0.032, 0.021, 0.201, and 0.119, respectively. And it is observed from an examination of the data presented in Table VIII that all of the ΔE values obtained by the proposed method are distinctly less than four other methods. This is because the proposed method considers the different weights of the visual perception in the R, G, and B channels of the color image, and adopts the B-R-G embedding principle to divide the embedding capacity of the R, G, and B channels. In addition, Table VIII shows that the method of Hou *et al.* [28] cannot achieve the required embedding capacity on the Kodim20. This is because the method of Hou *et al.* [28] only embedded the message into the R channel, recorded the auxiliary information into the B channel, and achieved grayscale invariance by adjusting the G channel. Hence, the method of Hou *et al.* [28] cannot achieve the required embedding capacity.

Fig. 11 shows the histogram distance [42] between the marked image and the cover image under different embedding capacities of the six standard images. A smaller histogram distance corresponds to greater similarity between the two images. However, the proposed method still maintains a large correlation between the marked image and the cover image when the size of the embedding messages increases. This also illustrates that the proposed method can obtained the marked image with a high visual quality.

As we know, the quality of an image strongly depends upon subjective assessment experiments to provide calibration data. The Mean Opinion Score (MOS) which is between [0, 5] can be used to reflect the perceived quality of the image. The higher the MOS value, the better of the image quality. Hence, we recruited 10 graduates from the Anhui university to score the quality of each marked images. Before the experiment, a short training showing the approximate range of quality of the images was also presented to each subject. Subjects were shown images in a random order and the randomization was different for each subject. Then subjects reported their judgments of quality according to each images number. Due to the subjective experiments are cumbersome to design and the time is constraint, we do our best to ensure that the testing environment was as close to the "real-world" as possible.

In order to compare subjective perception performance in all compared RDH methods in this paper, we choose six test images which are named as "Lena", "Airplane", "House", "Baboon", "Peppers" and "Barbara" to show the experiment results and subjective perception when embedding capacity is 50000bits. All 10 subjects test 30 marked images and give the average MOS score by 10 subjects in each image in Fig.12. From the point of subjective perception and MOS values, we can see that the marked images are all hardly to percept the difference between the original image and marked images in all RDH methods in this paper. In Table I, we have proved that it is hardly to percept the difference between the original image and marked images when ΔE less than 0.5. Hence, it is further proved that CIEDE2000 color-difference parameter ΔE can more accurately reflect the subtle changes in the images which subjective cannot percept.

VI. Conclusion

In this paper, we propose a high visual quality color image RDH scheme based on the B-R-G embedding principle and the CIEDE2000 assessment metric. Different from all traditional RDH methods, this paper proposes the use of CIEDE2000 as the image quality assessment metric due to its consistency with subjective perception. In addition, according to different visual perception in the three channels expressed by the brightness conversion formula, the B-R-G embedding principle is proposed to improve the visual quality of the marked color images. Experiments showed that the proposed method is superior to the state-of-the-art RDH methods for color images. In the future, the effect of combination of the channels on subjective perception in different image content can be further researched. In addition, the color image RDH method in encryption domain can be researched in the future.

References

[1] M. Asikuzzaman and M. R. Pickering, "An overview of digital video watermarking," *IEEE Trans. Circuits Syst. Video Technol.*, vol. 28, no. 9, pp. 2131–2153, Sep. 2018.

[2] X. Zhu, J. Ding, H. Dong, K. Hu, and X. Zhang, "Normalized correlation-based quantization modulation for robust watermarking," *IEEE Trans. Multimedia*, vol. 16, no. 7, pp. 1888–1904, Nov. 2014.

[3] A. Khan, A. Siddiqa, S. Munib, and S. A. Malik, "A recent survey of reversible watermarking techniques," *Inf. Sci.*, vol. 279, pp. 251–272, Sep. 2014, doi: 10.1016/j.ins.2014.03.118.

[4] I. A. Ansari, M. Pant, and C. W. Ahn, "SVD based fragile watermarking scheme for tamper localization and self-recovery," *Int. J. Mach. Learn. Cybern.*, vol. 7, no. 6, pp. 1225–1239, Dec. 2016.

[5] G. Paul, I. Davidson, I. Mukherjee, and S. S. Ravi, "Keyless dynamic optimal multi-bit image steganography using energetic pixels," *Multimedia Tools Appl.*, vol. 76, no. 5, pp. 7445–7471, Mar. 2017.

[6] J. Fridrich, M. Goljan, and R. Du, "Lossless data embedding for all image formats," *Proc. SPIE*, vol. 4675, pp. 572–583, Apr. 2002.

[7] M. U. Celik, G. Sharma, A. M. Tekalp, and E. Saber, "Lossless generalized-LSB data embedding," *IEEE Trans. Image Process.*, vol. 14, no. 2, pp. 253–266, Feb. 2005.

[8] C.-C. Chang, C.-C. Lin, C.-S. Tseng, and W.-L. Tai, "Reversible hiding in DCT-based compressed images," *Inf. Sci.*, vol. 177, no. 13, pp. 2768–2786, Jul. 2007.

[9] Z. Ni, Y.-Q. Shi, N. Ansari, and W. Su, "Reversible data hiding," *IEEE Trans. Circuits Syst. Video Technol.*, vol. 16, no. 3, pp. 354–362, Mar. 2006.

[10] M. Fallahpour and M. H. Sedaaghi, "High capacity lossless data hiding based on histogram modification," *IEICE Electron. Exp.*, vol. 4, no. 7, pp. 205–210, 2007.
[11] A. van Leest, M. van der Veen, and F. Bruekers, "Reversible image watermarking," in *Proc. Int. Conf. Image Process.*, vol. 2, Sep. 2003, p. 731.
[12] Y. Jia, Z. Yin, X. Zhang, and Y. Luo, "Reversible data hiding based on reducing invalid shifting of pixels in histogram shifting," *Signal Process.*, vol. 163, pp. 238–246, Oct. 2019.
[13] J. Tian, "Reversible data embedding using a difference expansion," *IEEE Trans. Circuits Syst. Video Technol.*, vol. 13, no. 8, pp. 890–896, Aug. 2003.
[14] D. M. Thodi and J. J. Rodriguez, "Expansion embedding techniques for reversible watermarking," *IEEE Trans. Image Process.*, vol. 16, no. 3, pp. 721–730, Mar. 2007.
[15] X. Gao, L. An, Y. Yuan, D. Tao, and X. Li, "Lossless data embedding using generalized statistical quantity histogram," *IEEE Trans. Circuits Syst. Video Technol.*, vol. 21, no. 8, pp. 1061–1070, Aug. 2011.
[16] X. Hu, W. Zhang, X. Li, and N. Yu, "Minimum rate prediction and optimized histograms modification for reversible data hiding," *IEEE Trans. Inf. Forensics Security*, vol. 10, no. 3, pp. 653–664, Mar. 2015.
[17] Y. Hu, H.-K. Lee, and J. Li, "DE-based reversible data hiding with improved overflow location map," *IEEE Trans. Circuits Syst. Video Technol.*, vol. 19, no. 2, pp. 250–260, Feb. 2009.
[18] W. Hong, T.-S. Chen, and C.-W. Shiu, "Reversible data hiding for high quality images using modification of prediction errors," *J. Syst. Softw.*, vol. 82, no. 11, pp. 1833–1842, Nov. 2009.
[19] X. Wu and N. Memon, "Context-based, adaptive, lossless image coding," *IEEE Trans. Commun.*, vol. 45, no. 4, pp. 437–444, Apr. 1997.
[20] L. Luo, Z. Chen, M. Chen, X. Zeng, and Z. Xiong, "Reversible image watermarking using interpolation technique," *IEEE Trans. Inf. Forensics Security*, vol. 5, no. 1, pp. 187–193, Mar. 2010.
[21] V. Sachnev, H. J. Kim, J. Nam, S. Suresh, and Y. Q. Shi, "Reversible watermarking algorithm using sorting and prediction," *IEEE Trans. Circuits Syst. Video Technol.*, vol. 19, no. 7, pp. 989–999, Jul. 2009.
[22] I.-C. Dragoi and D. Coltuc, "Local-prediction-based difference expansion reversible watermarking," *IEEE Trans. Image Process.*, vol. 23, no. 4, pp. 1779–1790, Apr. 2014.
[23] J. Wang, X. Chen, J. Ni, N. Mao, and Y. Shi, "Multiple histograms-based reversible data hiding: Framework and realization," *IEEE Trans. Circuits Syst. Video Technol.*, vol. 30, no. 8, pp. 2313–2328, Aug. 2020.
[24] Q. Chang, X. Li, Y. Zhao, and R. Ni, "Adaptive pairwise prediction-error expansion and multiple histograms modification for reversible data hiding," *IEEE Trans. Circuits Syst. Video Technol.*, early access, Jan. 29, 2021, doi: 10.1109/TCSVT.2021.3055612.
[25] J. Li, X. Li, and B. Yang, "Reversible data hiding scheme for color image based on prediction-error expansion and cross-channel correlation," *Signal Process.*, vol. 93, no. 9, pp. 2748–2758, Sep. 2013.
[26] B. Ou, X. Li, Y. Zhao, and R. Ni, "Efficient color image reversible data hiding based on channel-dependent payload partition and adaptive embedding," *Signal Process.*, vol. 108, pp. 642–657, Mar. 2015.
[27] H. Yao, C. Qin, Z. Tang, and Y. Tian, "Guided filtering based color image reversible data hiding," *J. Vis. Commun. Image Represent.*, vol. 43, pp. 152–163, Feb. 2017.
[28] D. Hou, W. Zhang, K. Chen, S.-J. Lin, and N. Yu, "Reversible data hiding in color image with grayscale invariance," *IEEE Trans. Circuits Syst. Video Technol.*, vol. 29, no. 2, pp. 363–374, Feb. 2019.
[29] A. D. Broadbent, "A critical review of the development of the CIE1931 RGB color-matching functions," *Color Res. Appl.*, vol. 29, no. 4, pp. 267–272, 2004.
[30] D. B. Judd and G. T. Yonemura, "CIE 1960 UCS diagram and the Müller theory of color vision," *J. Res. Nat. Bur. Standards Sect. A, Phys. Chem.*, vol. 74, no. 1, p. 23, Jan. 1970.
[31] A. R. Robertson, "The CIE 1976 color-difference formulae," *Color Res. Appl.*, vol. 2, no. 1, pp. 7–11, Mar. 1977.
[32] M. R. Luo, G. Cui, and B. Rigg, "The development of the CIE 2000 colour-difference formula: CIEDE2000," *Color Res. Appl.*, vol. 26, no. 5, pp. 340–350, 2001.
[33] G. M. Johnson and M. D. Fairchild, "A top down description of S-CIELAB and CIEDE2000," *Color Res. Appl.*, vol. 28, no. 6, pp. 425–435, Dec. 2003, doi: 10.1002/col.10195.
[34] N. Kawabata, "Multi-view 3D CG image quality evaluation and analysis for application procedure between H. 265/HEVC and watermarking," in *Proc. Int. Workshop Adv. Image Technol. (IWAIT)* Jan. 2018, pp. 1–4.
[35] N. Kawabata and M. Miyao, "Multi-view 3D CG image quality assessment for contrast enhancement based on S-CIELAB color space," *IEICE Trans. Inf. Syst.*, vol. 100, no. 7, pp. 1448–1462, 2017.
[36] J. Bai, T. Nakaguchi, N. Tsumura, and Y. Miyake, "Evaluation of image corrected by retinex method based on S-CIELAB and gazing information," *IEICE Trans. Fundamentals Electron., Commun. Comput. Sci.*, vol. 89, no. 11, pp. 2955–2961, Nov. 2006, doi: 10.1093/ietfec/e89-a.11.2955.
[37] K. Hirai, J. Tumurtogoo, A. Kikuchi, N. Tsumura, T. Nakaguchi, and Y. Miyake, "Video quality assessment using spatio-velocity contrast sensitivity function," *IEICE Trans. Inf. Syst.*, vol. 93, no. 5, pp. 1253–1262, 2010.
[38] M. A. Erle, M. J. Schulte, and B. J. Hickmann, "Decimal floating-point multiplication via carry-save addition," in *Proc. 18th IEEE Symp. Comput. Arithmetic (ARITH)*, Jun. 2007, pp. 46–55.
[39] *2020 the USE-SIPI Image Database*. [Online]. Available: http://sipi.usc.edu/database/
[40] *2020 Laboratory for Image & Video Engineering*. [Online]. Available: http://live.ece.utexas.edu/research/quality
[41] *2020 Kodak Lossless True Color Image Suite*. [Online]. Available: http://r0k.us/graphics/kodak/
[42] S.-H. Cha and S. N. Srihari, "On measuring the distance between histograms," *Pattern Recognit.*, vol. 35, no. 6, pp. 1355–1370, Jun. 2002.

Yang Yang received the M.S. degree from Anhui University, in 2007, and the Ph.D. degree from the University of Science and Technology of China, in 2013.

She was a Post-Doctoral Researcher with the University of Science and Technology of China, from 2015 to 2018. She is currently an Associate Professor with Anhui University. Her research interests include reversible information hiding, privacy protect, and image quality assessment.

Tianrui Zou is currently pursuing the master's degree with the School of Electronics and Information Engineering, Anhui University, China. His research interests include reversible data hiding for color images and privacy protect.

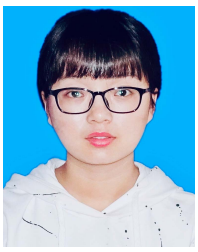

Genyan Huang is currently pursuing the master's degree with the School of Electronics and Information Engineering, Anhui University, China. Her research interests include reversible data hiding and privacy protect.

Weiming Zhang received the M.S. and Ph.D. degrees from the Zhengzhou Information Science and Technology Institute, Zhengzhou, China, in 2002 and 2005, respectively.

He is currently a Professor with the School of Information Science and Technology, University of Science and Technology of China. His research interests include multimedia security, information hiding, and privacy protection.